ORNL/TM-7658
Dist. Category UC-20 g

Contract No. W-7405-eng-26

FUSION ENERGY DIVISION

ORNL/TM--7658

DE82 008146

NEUTRAL-BEAM DEPOSITION IN LARGE, FINITE-BETA NONCIRCULAR TOKAMAK PLASMAS

R. M. Wieland

Computer Sciences

and

W. A. Houlberg

Fusion Energy Division

Date Published - February 1982

NOTICE **This document contains information of a preliminary nature. It is subject to revision or correction and therefore does not represent a final report.**

Prepared by the
OAK RIDGE NATIONAL LABORATORY
Oak Ridge, Tennessee 37830
operated by
UNION CARBIDE CORPORATION
for the
DEPARTMENT OF ENERGY

CONTENTS

ABSTRACT

A "parametric" pencil beam model is introduced for describing the attenuation of an energetic neutral beam moving through a tokamak plasma. The nonnegligible effects of a finite beam cross section and noncircular shifted plasma cross sections are accounted for in a simple way by using a smoothing algorithm dependent linearly on beam radius and by including information on the plasma flux surface geometry explicitly. The model is benchmarked against more complete and more time-consuming two-dimensional Monte Carlo calculations for the case of a large D-shaped tokamak plasma with minor radius a = 120 cm and elongation b/a = 1.6. Deposition profiles are compared for deuterium beam energies of 120-150 keV, central plasma densities of 8×10^{13}-2×10^{14} cm^{-3}, and beam orientation ranging from perpendicular to tangential to the inside wall.

1. INTRODUCTION

Neutral beam heating of tokamak reactor plasmas has been the subject of extensive study[1-3] over the past several years, not only as a necessary means to overcome the inherent limitations of pure ohmic heating but also as a possible means of achieving a sustained current drive.[4-6] As higher plasma betas are achieved, it becomes important to correctly model the higher order geometrical effects imposed on the fast ion deposition profile H(r) by the resulting distorted plasma cross sections. As we shall show, noncircular, shifted plasma flux surfaces can significantly alter these deposition profiles from what they would be in a corresponding low-beta, circular, concentric case.

The physics behind the attenuation of an energetic neutral beam moving through a hot, dense plasma is well known. What we consider here is a "parametric" model for this process where the finite beam and noncircular plasma cross sections are accounted for. After writing the analytic description of a pencil beam, we introduce an algorithm which includes these finite effects. We then benchmark the model against more exact Monte Carlo calculations for a number of geometries, beam energies, and beam radii. The limitations inherent in our approach are pointed out and balanced against the extremely fast computer execution time of our code, vis-a-vis possible incorporation into plasma transport codes.

2. PROBLEM DEFINITION

2.1. Plasma/Beam Parameters

In order to obtain a fast ion deposition profile, it is necessary to specify several key parameters related to the plasma and to the beam. Since plasma temperature and density are expected to be constant on surfaces of constant poloidal or toroidal flux for a plasma in equilibrium, all the key geometric plasma parameters relate to a specification of these flux contours in the R-Z plane. Shown in Fig. 1 is a set of such contours for an FED/INTOR-sized plasma with a major radius to the geometric center of R_G = 474.6 cm, a major radius to the magnetic axis of R_o = 512.9 cm, and a minor radius in the midplane of a_o = 123 cm. For the equilibrium case shown, the finite beta results in a shifting of the flux surfaces outward as one moves toward the magnetic axis, with a resulting steeper gradient in all plasma parameters toward the outside of the plasma. Significant elongation, b_o/a_o = 1.5, and triangularity, c_o/a_o = 0.5, are also evident in the figure, resulting in a modulation of the differential volumes from a simple circular case. Also shown in Fig. 1 is a horizontal projection of a neutral beam path for a beam radius of 20 cm. This side view illustrates the coupling between the finite plasma elongation and the beam path component parallel to but displaced from the midplane of the torus. Note that larger elongations allow better "penetration" for the extreme off-plane particles. This is one of the finite beam effects mentioned earlier. A top view of the plasma-beam system (Fig. 2) highlights the various beam trajectories considered here, with a

convenient trajectory parameter designated by the distance of closest approach, R_B, of the beam path to the center of the torus.

In order to reduce this three-dimensional (3-D) system to a workable one-dimensional (1-D) model, we employ the grid scheme shown in Fig. 3. The usual 1-D radial grid is replaced by an effective radius coordinate r that is defined to lie between two parallel midplane grids R_{IN} and R_{OUT}. The latter correspond to the intersection of the plasma flux contours with the midplane of the torus, inside and outside of the magnetic axis, respectively. This scheme allows for a 1-D representation of shifted flux surfaces. The arbitrary shape of each flux surface is accounted for by an array of differential volume elements (DVOL) that represent the volume between adjacent poloidal flux contours. This metric makes it possible to collapse the 3-D plasma onto the midplane, as it were, resulting in a convenient 1-D representation of the plasma. While information has been lost on the region of beam-plasma interaction off of the midplane, it is possible to reconstruct this in an ad hoc way by taking a pencil beam of infinitesimal cross section and broadening the resulting deposition profile parametrically in terms of the finite beam geometry.

2.2. Fast Ion Deposition Profile--H(r)

The fast ion deposition profile H(r), or $H(\psi)$, is defined as a dimensionless shape factor that is related to the fast ion birth rate by the following expression:

$$\dot{n}_f(r) = \frac{I_o/e}{V} H(r) \qquad (1)$$

where $\dot{n}_f$ is the rate ($cm^{-3} \cdot s^{-1}$) at which fast ions are born as a result of the neutral beam-plasma interaction, I_o/e is the neutral particle current, and V is the total volume of the plasma. The total fraction of incident beam ionized by the plasma, then, is

$$\frac{\int \dot{n}_f dV}{I_o/e} = \frac{1}{V} \int H(r) dV \tag{2}$$

For an idealized pencil beam, the relative attenuation in passing through a "cell" of differential volume ΔV is

$$\Delta I = I_o \left[1 - \exp\left(\frac{-n_o \langle \sigma v \rangle}{v_o} \Delta \ell\right)\right] \tag{3}$$

where ΔI is the decrement in intensity due to ionization, I_o is the neutral particle intensity incident on the cell, n_o is the background plasma density, and $\langle \sigma v \rangle$ is the ionization rate for a neutral particle moving with velocity v_o through a Maxwellian plasma distribution. The path length through the cell $\Delta \ell$ depends on the incident beam trajectory (Fig. 2). The ionization rate $\langle \sigma v \rangle$ represents a contribution from charge exchange (σ_{cx}), electron impact ionization (σ_{ei}), and ion impact ionization (σ_{ii}), so that

$$\sigma = \sigma_{cx} + \sigma_{ei} + \sigma_{ii}$$

These cross sections have been tabulated for atomic hydrogen beams

traversing atomic hydrogen;[7,8] they are easily applied to other species by expressing them in terms of hydrogenic velocities.

By following the trajectory of the beam across the plasma, using Eq. (3), H(r) is built up by integration:

$$H(r) \simeq \sum_i \Delta H_i$$

where

$$\Delta H_i = \left[\frac{(\Delta I_o)_i}{DVOL_i}\right] V$$

and the summation is taken over each cell (designated by the subscript i) traversed. The resulting H(r) is entirely local, in that it only considers the birth point of the fast ion, and not the subsequent "smearing" of its effective radial position due to finite orbit and drift effects. The latter effects have been considered in detail by Fowler et al.,[9] and are easily calculated within the context of a Monte Carlo type code; they are expected to be appreciable, however, only in cases involving large orbits, such as counterinjection or for those injection trajectories (nearly) perpendicular to the field lines.

3. MODELING FINITE BEAM EFFECTS

The parameters that are included under the umbrella of finite beam effects are factors such as beam radius, arbitrary beam cross section and profile, divergence, and focus. A complete consideration of all these real beam parameters requires a Monte Carlo type treatment although in practice the experimental uncertainty attached to many of these parameters makes such time-consuming calculations unwarranted, particularly when extrapolating to larger systems. Another approach is to model the finite cross-section beam by a collection of pencil beamlets suitably distributed over the profile.[10] This represents a considerable savings in computation time, although off-plane trajectories still present a problem that requires careful geometrical computation. In the approach we describe here, we remain on the midplane by using a single pencil beam, redistributing the resulting deposition profile H(r) by a smoothing algorithm that takes into account various constraints imposed on the profile by the physics and geometry of the problem. The correct "smoothing" is chosen by a careful comparison with Monte Carlo type calculations which are taken to be the standard against which we benchmark our results.

The smoothing algorithm contains a single parameter, the smoothing radius R_{SM}, such that over the range $r = 0 - R_{SM}$, H(r) is replaced by $\hat{H}(r)$, where $\hat{H}(r)$ is obtained from a cubic that satisfies the following conditions:

(1) $\frac{d\hat{H}}{dr} = 0$ at $r = 0$

(2) $\int_0^{R_{SM}} \hat{H} dV = \int_0^{R_{SM}} H dV$

(3) $\hat{H} = H$ at $r = R_{SM}$

(4) $\frac{d\hat{H}}{dr} = \frac{dH}{dr}$ at $r = R_{SM}$

This procedure is motivated by the knowledge that H(r) for a pencil beam has a singularity at r = 0 and that this singularity can be integrated (i.e., it vanishes for a finite beam). Condition (1) above preserves the flattening of the profile that results from an exact integration. Condition (2) ensures that particle number is conserved in the deposition region, and conditions (3) and (4) preserve continuity in the function and its derivative at the matching point R_{SM}. Figure 4 illustrates the H(r) profiles which result from a varying R_{SM}. Note that only the central region of each profile is plotted.

The two cases represent inward and outward peaked profiles typical of good penetration and strong edge absorption, respectively. As R_{SM} is increased, the central singularity is redistributed over the smoothing region, with a resulting decrease of H(r) near the origin. Changes in R_{SM} have no noticeable effect on the outer 90% of the profile.

Earlier studies have been made with concentric, circular plasma geometries to determine an optimum parameterization for R_{SM} as a function of the various finite beam variables. Using the circular Monte Carlo beam deposition code FREYA[11] as a benchmark, it was found[12] that the only significant parameter dependence was on beam radius, all the other factors being only of weak influence. The

results of this study are summarized in Fig. 5, where the best-fit smoothing radius R_{SM} is plotted against the beam radius for a number of injection energies and for two injection trajectories. The two plasma geometries considered are a PLT-sized device (R_o = 130 cm, a_o = 45 cm) and a TFTR-sized device (R_o = 248 cm, a_o = 85 cm). Detailed comparisons of the resulting H(r) profiles against the Monte Carlo standard are shown in Figs. 6 and 7. These studies indicate that for over a wide range of parameters, a choice of R_{SM} equal to twice the beam radius is an excellent choice to provide good reproductory H(r) profiles.

4. HIGH-BETA EFFECTS

4.1. Goals

Up to this point we have only considered in detail circular, nonshifted plasmas (i.e., $\langle\beta\rangle \approx 0$). In this section, we will examine the applicability of our model to finite beta plasmas, i.e., those which exhibit noncircular, shifted flux contours. Specifically, we are interested in showing that the model parameterizations obtained in the previous section also apply to these more realistic cases and that the grid system we use is capable of modeling the more complex geometry. Having done this, we will be in a position to examine straightforwardly the specific effects that finite beta imposes on the resulting deposition profile.

4.2. A High-Beta Equilibrium

The high-beta equilibrium case that we will study here is shown in Fig. 1. The elongation and triangularity of the outermost flux surface are $b_o/a_o = 1.5$ and $c_o/a_o = 0.5$, respectively. The outward shift of the magnetic axis, $\delta_o \sim 38$ cm, is fully 30% of the minor radius. Volume-averaged beta toroidal is 6.5%, with beta poloidal ~2.9. We consider here two cases represented by the same equilibrium: a high density, low penetration case ($n_{e_o} \sim 2 \times 10^{14}$ cm^{-3}) and a lower density, high penetration case ($n_{e_o} \sim 8 \times 10^{13}$ cm^{-3}). As before, these lead to significant differences in the shape of the deposition profile and test the versatility of our parameterization using R_{SM}.

4.3. Benchmark Results

In order to benchmark our H(r) profiles, we compare them with the results of the noncircular geometry Monte Carlo code NFREYA,[9] with and without bounce averaging. The reference neutral beam used is deuterium, with an infinite focal length and zero divergence, a circular cross section, uniform profile, and a radius of 20 cm (R_b). The beam trajectories are those shown in Fig. 2, all incident on the plasma along the midplane of the torus. Two beam energies are studied: 120 keV and 150 keV. The NFREYA calculation is fully three-dimensional, using all the equilibrium information given in Sect. 4.2, whereas our code BEAM distills this input by considering only midplane projections with additional information stored in the RIN/ROUT and DVOL arrays.

Figures 8-11 show a comparison of the resulting H(r) from BEAM versus the corresponding output from NFREYA for a number of cases. In each case, $R_{SM}/R_b = 2$, with no other free parameters; the effective smoothing radius for the noncircular geometry is defined as the radius at which the cross-sectional area of the plasma is four times the cross-sectional area of the beam. The bounce-averaged results from NFREYA are also included for the sake of completeness, although in the cases shown here the effects are insignificant. The data for the innermost cell in the NFREYA calculations are plotted at the half radius for the cell while the data for the beam calculations are plotted at the origin. Thus, the endpoints of the plots in both cases represent H(0). The agreement between the two codes is almost exact, whether for good penetration (Figs. 8 and 9) or for poor penetration (Figs. 10 and 11). In each case, only the full energy component of the

beam is shown. Figure 12 shows no deterioration in the agreement between codes when the lower half- and third-energy components are considered.

4.4. Specific High-Beta Effects

In order to isolate the high-beta effects of shifted flux surfaces on the attendant H(r) profile, we consider here the case of an "equivalent" zero-beta equilibrium that is constructed by replacing the D-shaped flux surfaces in Fig. 1 with concentric ellipses of elongation ε centered at the same major radius, R_G = 474.6 cm. The value of ε is chosen so as to preserve the total volume of the plasma. A comparison of the resulting H(r) for this case with the H(r) for the full finite-beta case shown in Fig. 1 is presented in Fig. 13. The outward shift of the flux surfaces in the finite-beta case shortens the optical path length of the beam to the magnetic axis, leading to significantly increased penetration, even at 40 keV. The greatest advantage of the shift is to reduce the beam energy requirements for finite-beta, beam-driven plasmas since the energy and path length for a given degree of penetration are approximately related by $E_o \propto \ell$.

5. PENCIL BEAM VERSUS MONTE CARLO

The main advantage that the pencil beam model has over the Monte Carlo approach is in the large savings in computation. When incorporated into a larger code that uses it repetitively, this translates directly into a savings in computer time. On the CDC 7600, for example, running both codes in optimum fashion, the BEAM code is roughly 50 times faster than NFREYA. The limitations for the former have to be recognized, however; BEAM cannot treat diffuse beam trajectories off the midplane nor can it account for nonlocal "bounce" effects when they are important. Finally, the smoothing algorithm parameterization of R_{SM} is reasonable only for those cases where $R_B << a_o$. This is not the case, for example, in a device such as ISX-B. Furthermore, the optimal parameterization of $R_{SM} \approx 2R_B$, presented here, must be reevaluated for departures from circular, constant profile beam cross sections.

6. CONCLUSIONS

We have shown that the pencil beam model can be successfully modified to treat not only finite beams but also their interaction with finite-beta plasmas. A single parameter is sufficient to accurately reproduce more detailed, Monte Carlo H(r) deposition profiles, and the dependence of this parameter on beam and plasma variables has been demonstrated to reduce to simple linear relationship with the beam radius. Furthermore, the outward shift in magnetic axis due to finite-beta considerations has a marked influence on H(r) deposition profiles, increasing the penetration significantly over large regions of the beam-plasma interaction.

ACKNOWLEDGMENT

The authors are grateful to D. J. Strickler for providing the equilibrium data used in Sect. 4.2.

REFERENCES

1. J. G. Cordey, in Proceedings of Physics of Plasmas Close to Thermonuclear Fusion (Varenna, Italy, 1979) Vol. I, p. 359.

2. J. A. Holmes, J. A. Rome, W. A. Houlberg, Y-K. M. Peng, and S. J. Lynch, Nucl. Fusion 20, 59 (1980).

3. W. A. Houlberg, S. E. Attenberger, and A. T. Mense, Nucl. Fusion 20, 811 (1980).

4. T. Ohkawa, Nucl. Fusion 10, 185 (1970).

5. J. G. Cordey, E. M. Jones, D. F. H. Start, A. R. Curtis, and I. P. Jones, Nucl. Fusion 19, 249 (1979).

6. S. P. Hirshman, Phys. Fluids 23, 1238 (1980).

7. R. L. Freeman and E. M. Jones, "Atomic Collisions in Plasma Physics Experiments," Culham Laboratory Report CLM-R 137, 1974.

8. A. C. Riviere, Nucl. Fusion 11, 363 (1971).

9. R. H. Fowler, J. A. Holmes, and J. A. Rome, "NFREYA - A Monte Carlo Beam Deposition Code for Noncircular Tokamak Plasmas," Oak Ridge National Laboratory Report ORNL/TM-6845, 1979.

10. J. A. Rome, J. D. Callen, and J. F. Clarke, Nucl. Fusion 14, 141 (1974).

11. G. G. Lister, D. E. Post, and R. Goldston, in Proceedings of 3rd Symposium on Plasma Heating in Toroidal Devices (Varenna, Italy, 1976), p. 303.

12. R. M. Wieland, W. A. Houlberg, and A. T. Mense, "A Comparison of Beam Deposition for Three Neutral Beam Injection Codes," Oak Ridge National Laboratory Report ORNL/TM-6550, 1979.

FIGURE CAPTIONS

Fig. 1. Projection of the midplane beam path (beam diameter = 40 cm) on the poloidal plane. The dashed contour indicates the magnitude of the smoothing radius used in the calculations. R_M is the coordinate of the magnetic axis, R_o the plasma major radius, and a_o the minor radius. The elongation of the plasma boundary is $\varepsilon = b_o/a_o = 1.5$ and the triangularity is $\delta = c_\ell/a_o = 0.53$. δ_o indicates the magnitude of the magnetic axis shift.

Fig. 2. Midplane projection of the various beam trajectories discussed in the text.

Fig. 3. Schematic view of the mesh geometry.

Fig. 4. The variation of H(r) (BEAM) with smoothing radius R_{SM}.

Fig. 5. The variation of R_{SM}/R_{BEAM} with beam radius for the various parameters indicated.

Fig. 6. H(r) profiles from BEAM (solid) and FREYA (dashed) for four typical TFTR cases.

Fig. 7. H(r) profiles from BEAM (solid) and FREYA (dashed) for four typical PLT cases.

Fig. 8. H(r) profiles from BEAM (solid) and NFREYA (dashed) for four beam trajectories at E_o = 120 keV and $n_{eo} = 8 \times 10^{13}$ cm^{-3}.

Fig. 9. H(r) profiles from BEAM (solid) and NFREYA (dashed) for four beam trajectories at E_o = 150 keV and $n_{eo} = 8 \times 10^{13}$ cm^{-3}.

Fig. 10. H(r) profiles from BEAM (solid) and NFREYA (dashed) for four beam trajectories at E_o = 120 keV and $n_{eo} = 2 \times 10^{14}$ cm^{-3}.

Fig. 11. H(r) profiles from BEAM (solid) and NFREYA (dashed) for four beam trajectories at E_o = 150 keV and $n_{eo} = 2 \times 10^{14}$ cm^{-3}.

Fig. 12. H(r) comparison for all three beam energy components at E_o = 120 keV and $n_{eo} = 2 \times 10^{14}$ cm^{-3}.

Fig. 13. A comparison of H(r) (for all three beam energy components) at two different $\langle\beta\rangle$ values.

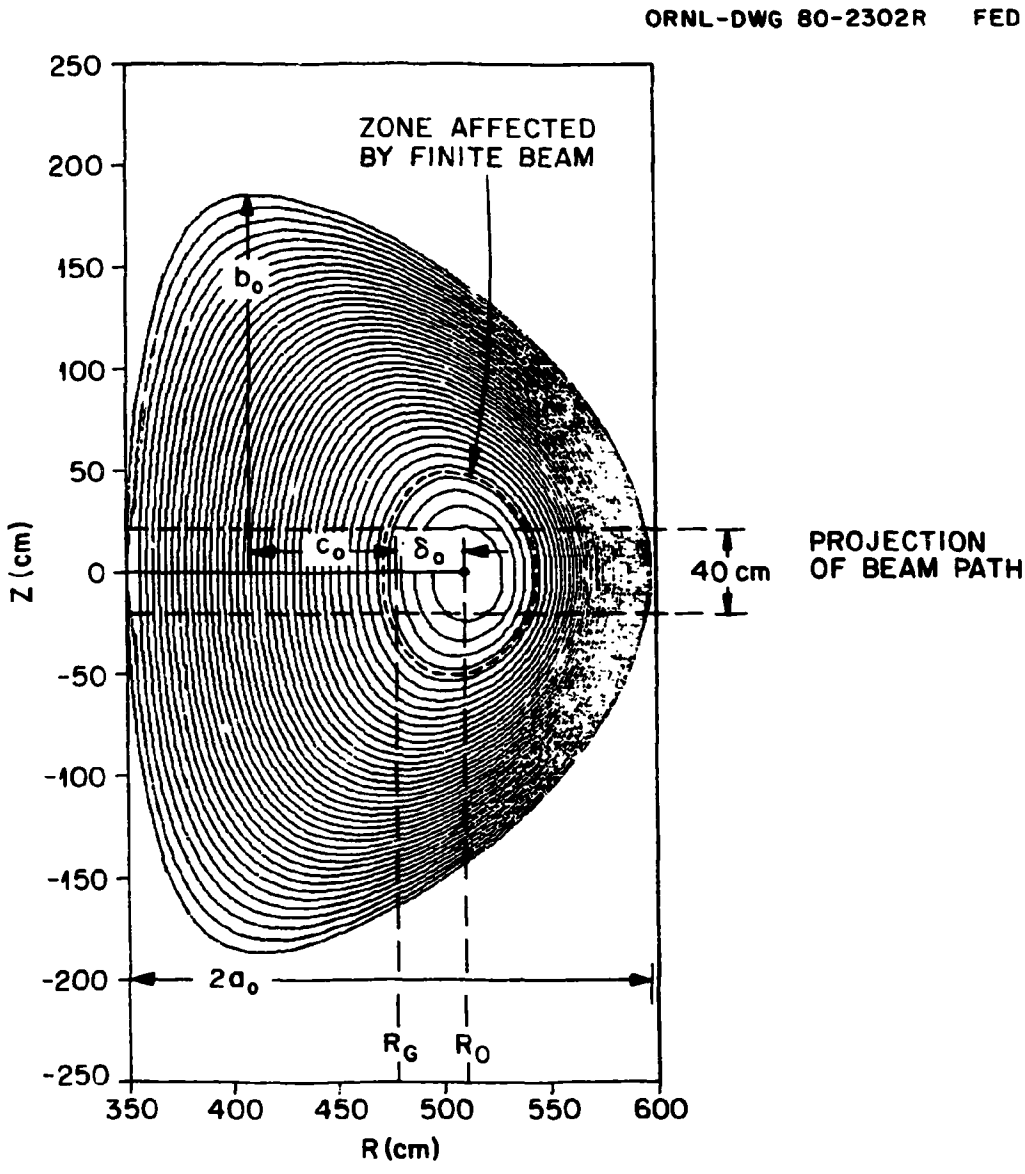
ORNL-DWG 80-2302R FED
ZONE AFFECTED
BY FINITE BEAM
b_o
c_o
δ_o
40 cm
PROJECTION
OF BEAM PATH
$2a_o$
R_G
R_O
Z (cm)
R (cm)
250
200
150
100
50
0
-50
-100
-150
-200
-250
350
400
450
500
550
600

Fig. 1.

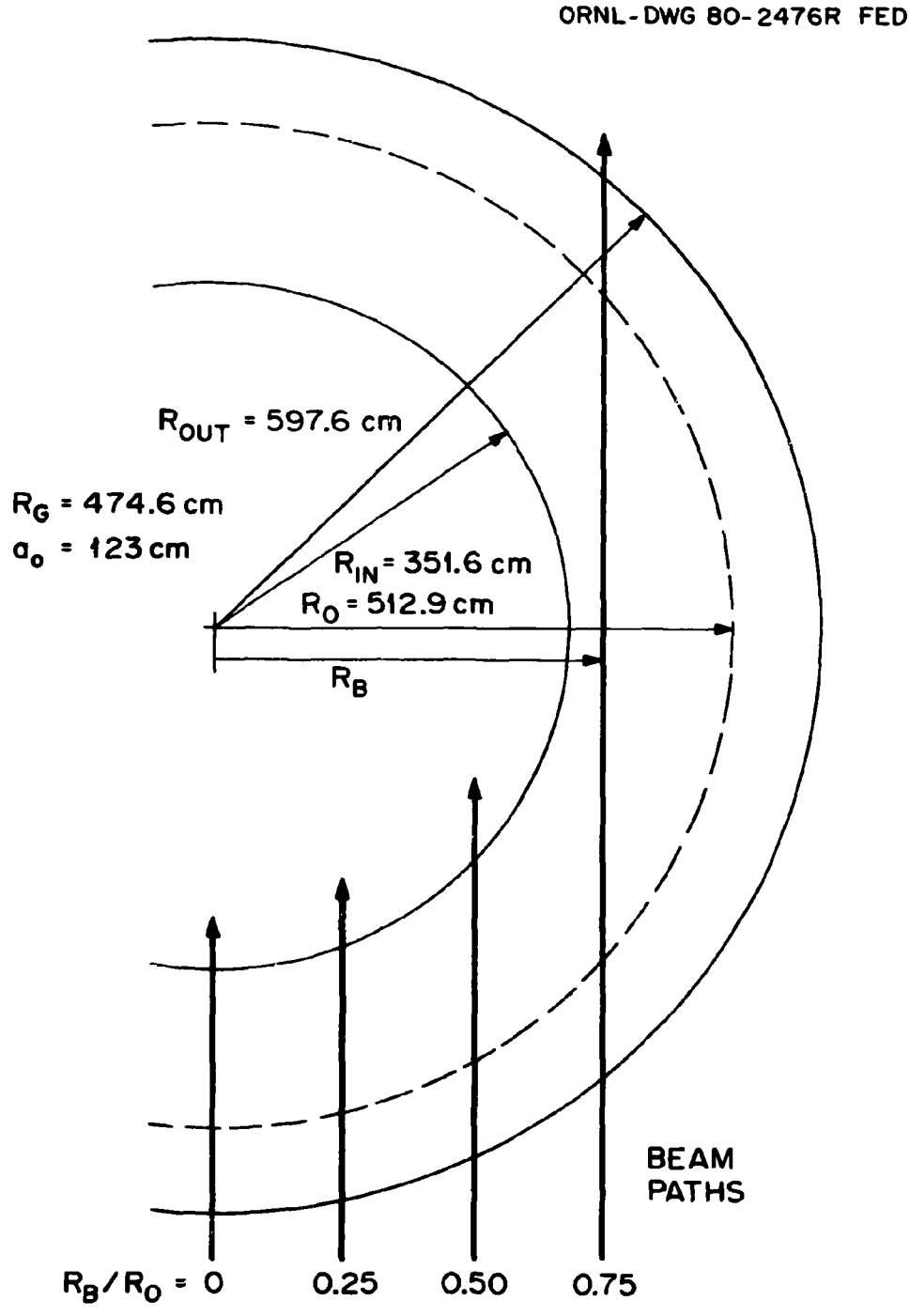
ORNL-DWG 80-2476R FED
R_{OUT} = 597.6 cm
R_G = 474.6 cm
a_o = 123 cm
R_{IN} = 351.6 cm
R_O = 512.9 cm
R_B
BEAM PATHS
R_B/R_O = 0
0.25
0.50
0.75

Fig. 2.

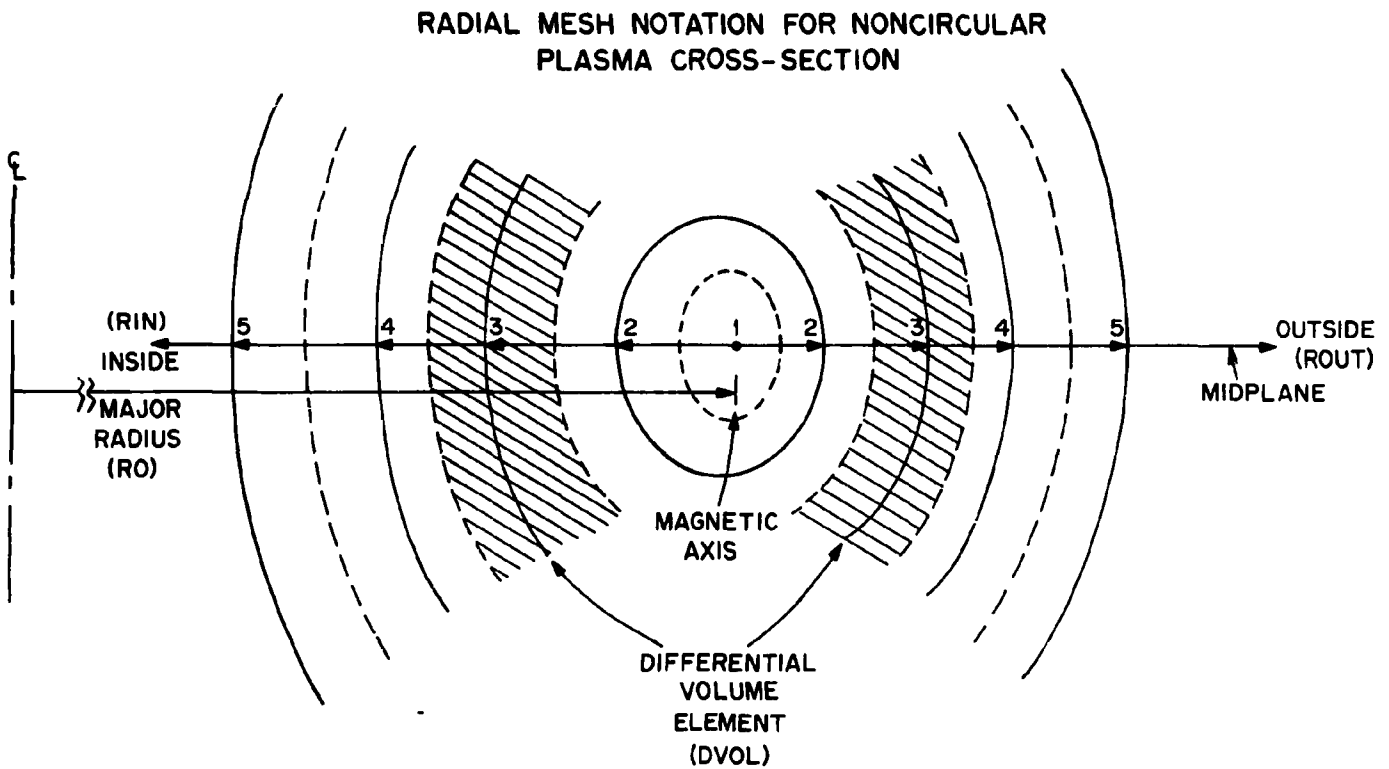
RADIAL MESH NOTATION FOR NONCIRCULAR PLASMA CROSS-SECTION
℄
(RIN)
INSIDE
MAJOR
RADIUS
(RO)
5
4
3
2
1
2
3
4
5
OUTSIDE
(ROUT)
MIDPLANE
MAGNETIC
AXIS
DIFFERENTIAL
VOLUME
ELEMENT
(DVOL)

Fig. 3.

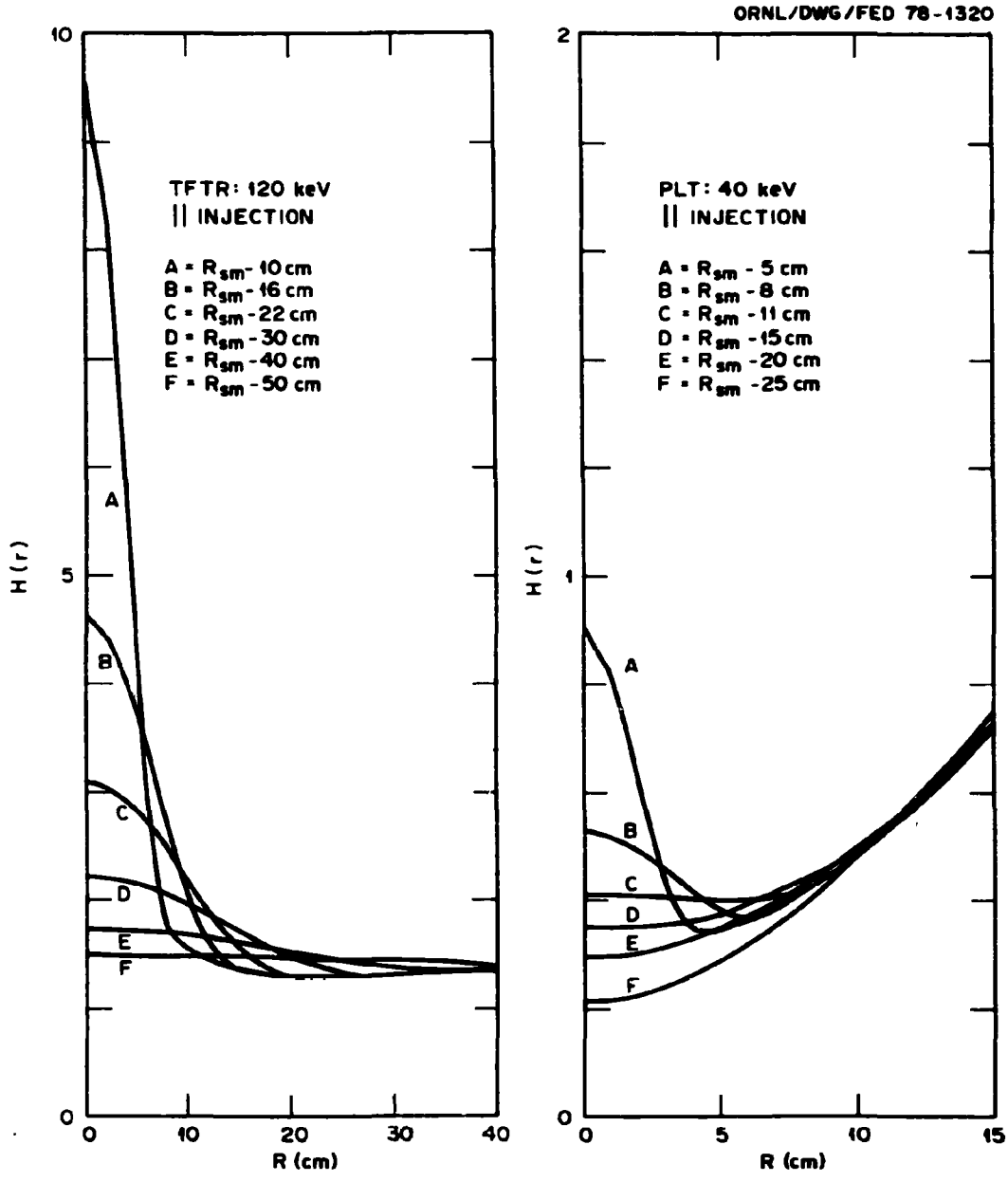
ORNL/DWG/FED 78-1320
TFTR: 120 keV
|| INJECTION
A = Rsm - 10 cm
B = Rsm - 16 cm
C = Rsm - 22 cm
D = Rsm - 30 cm
E = Rsm - 40 cm
F = Rsm - 50 cm
H(r)
R (cm)
PLT: 40 keV
|| INJECTION
A = Rsm - 5 cm
B = Rsm - 8 cm
C = Rsm - 11 cm
D = Rsm - 15 cm
E = Rsm - 20 cm
F = Rsm - 25 cm
H(r)
R (cm)

Fig. 4.

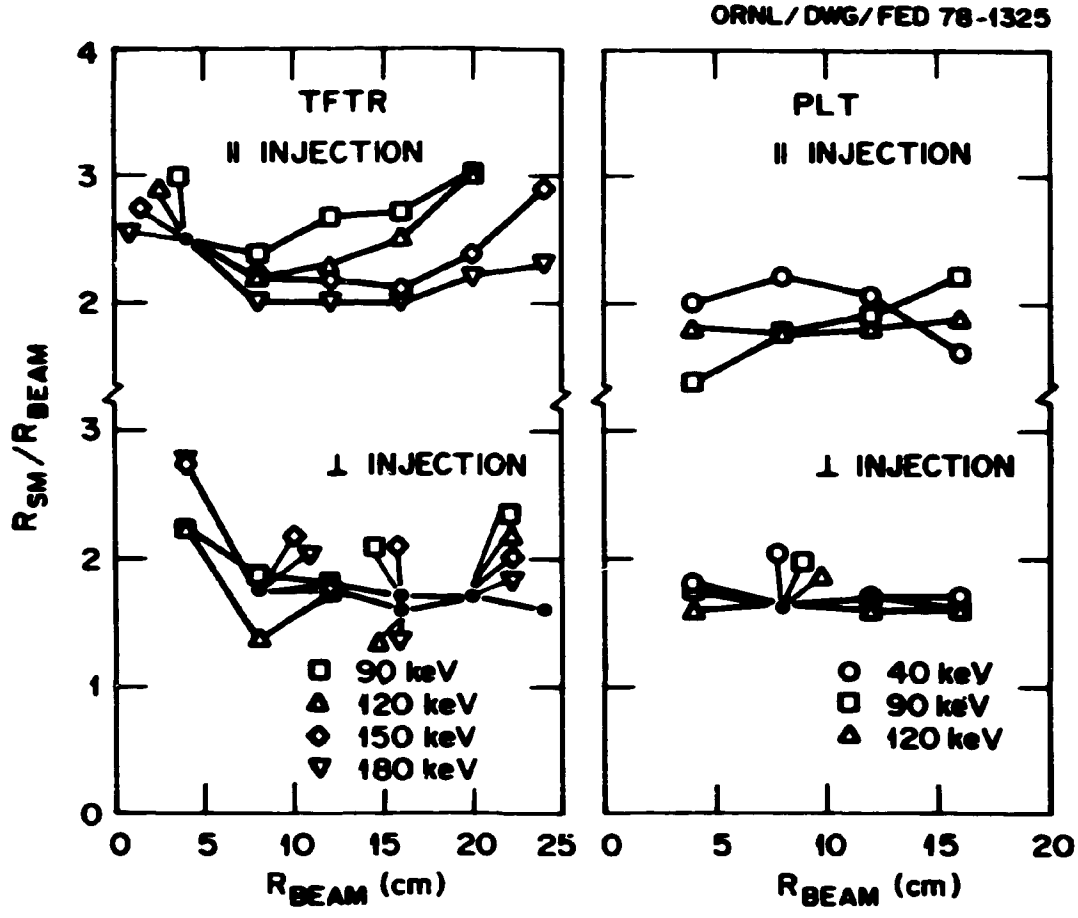
ORNL/DWG/FED 78-1325
TFTR
II INJECTION
⊥ INJECTION
90 keV
120 keV
150 keV
180 keV
PLT
II INJECTION
⊥ INJECTION
40 keV
90 keV
120 keV
R_{SM}/R_{BEAM}
R_{BEAM} (cm)
R_{BEAM} (cm)

Fig. 5.

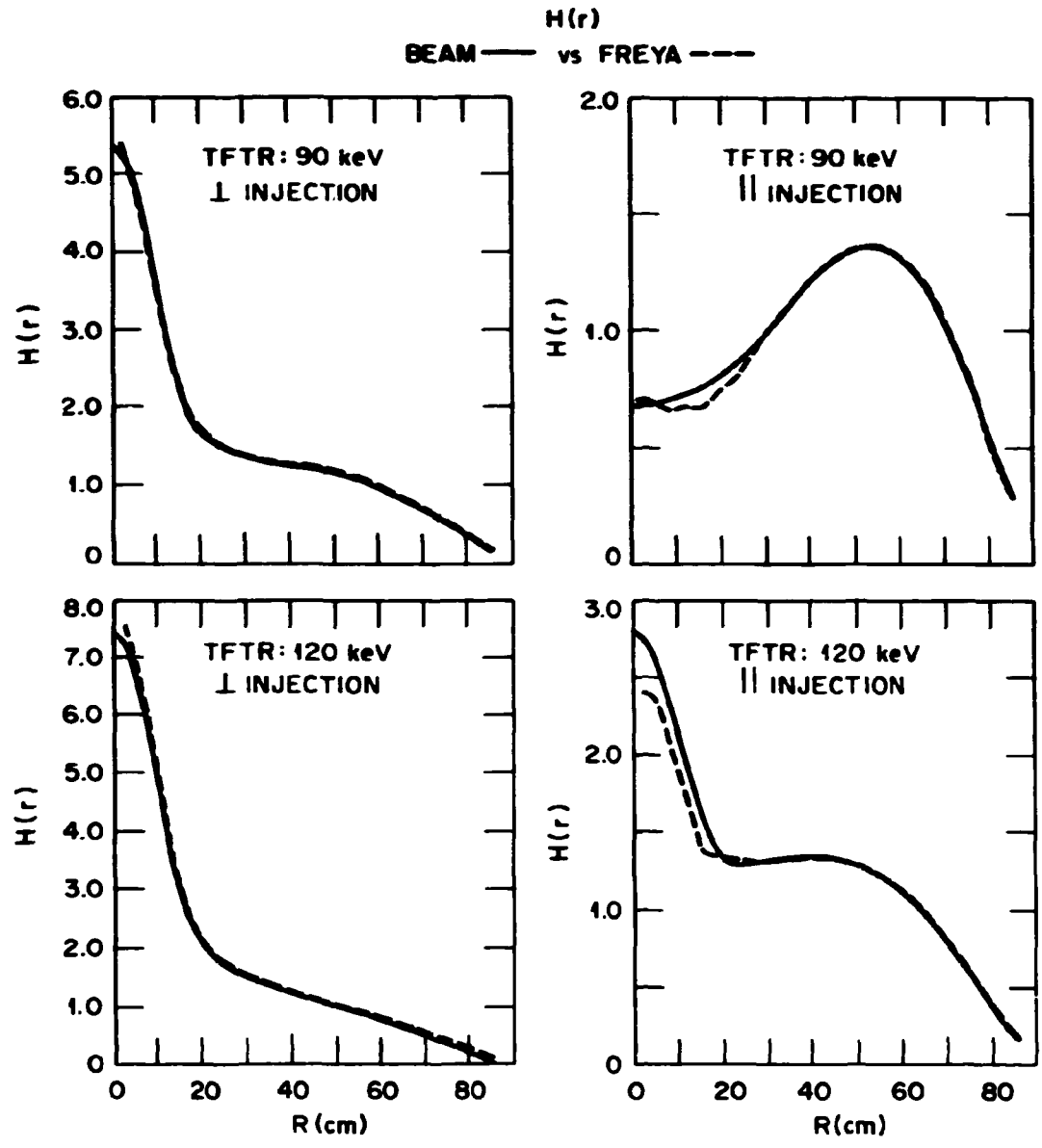
ORNL/DWG/FED 78-1323
H(r)
BEAM —— vs FREYA ---
TFTR: 90 keV
⊥ INJECTION
TFTR: 90 keV
|| INJECTION
TFTR: 120 keV
⊥ INJECTION
TFTR: 120 keV
|| INJECTION
H(r)
R(cm)
0
20
40
60
80

Fig. 6.

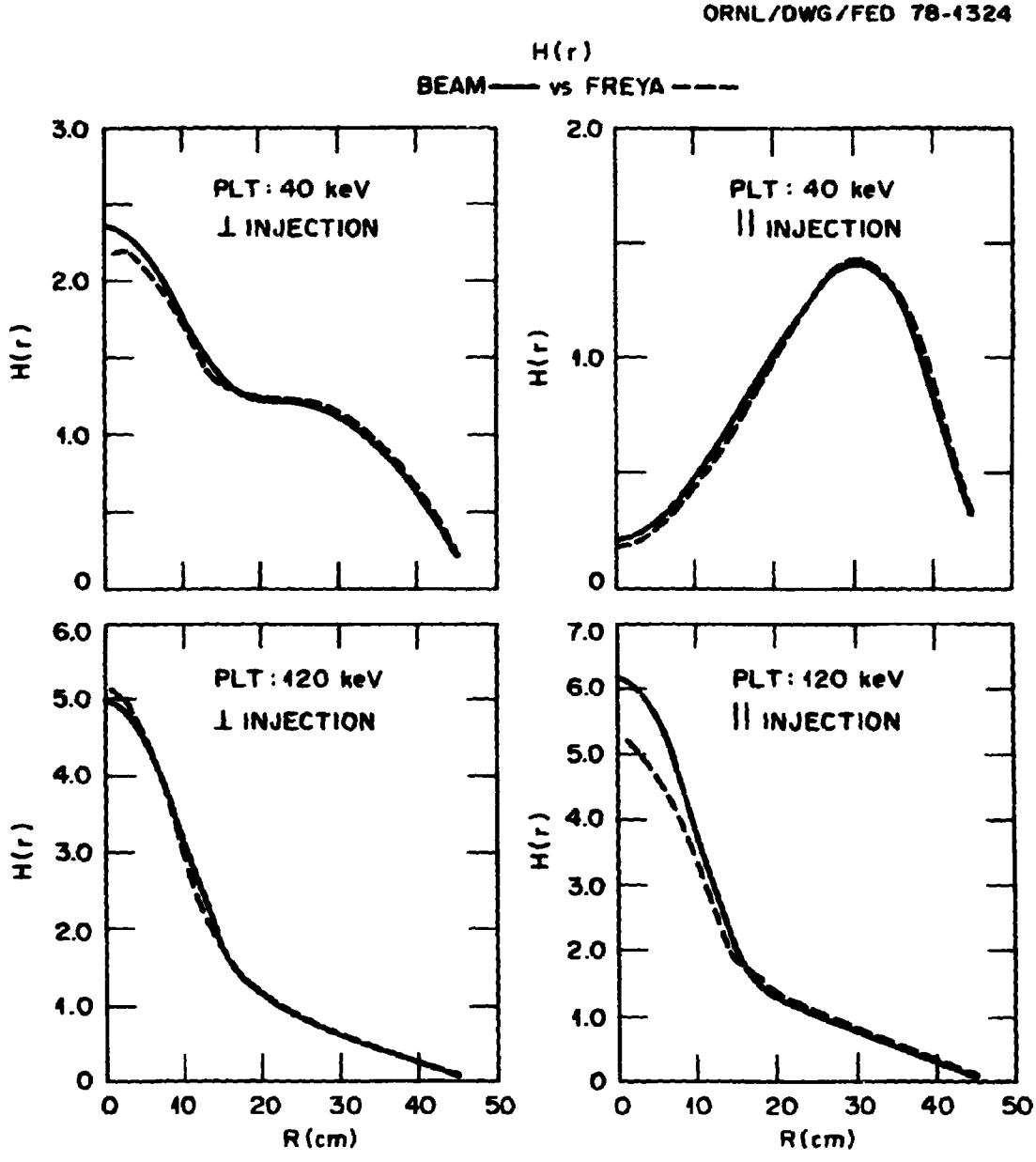
ORNL/DWG/FED 78-1324
H(r)
BEAM—— vs FREYA - - -
PLT: 40 keV
⊥ INJECTION
PLT: 40 keV
|| INJECTION
PLT: 120 keV
⊥ INJECTION
PLT: 120 keV
|| INJECTION
H(r)
R(cm)

Fig. 7.

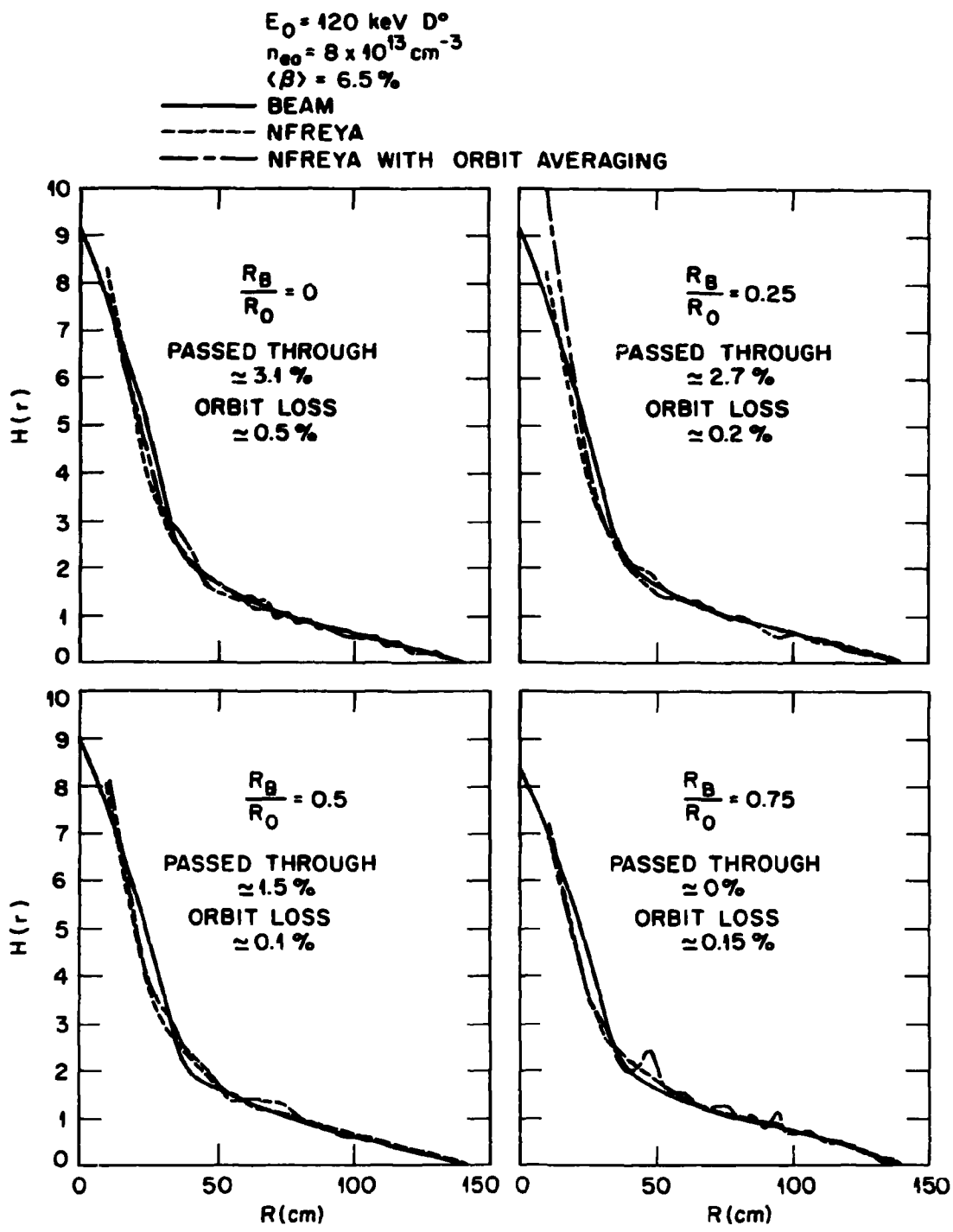
ORNL-DWG 80-2399 FED
E_0 = 120 keV D°
n_{e0} = 8 x 10^{13} cm^{-3}
⟨β⟩ = 6.5 %
BEAM
NFREYA
NFREYA WITH ORBIT AVERAGING
$\frac{R_B}{R_0}$ = 0
PASSED THROUGH
≃ 3.1 %
ORBIT LOSS
≃ 0.5 %
$\frac{R_B}{R_0}$ = 0.25
PASSED THROUGH
≃ 2.7 %
ORBIT LOSS
≃ 0.2 %
$\frac{R_B}{R_0}$ = 0.5
PASSED THROUGH
≃ 1.5 %
ORBIT LOSS
≃ 0.1 %
$\frac{R_B}{R_0}$ = 0.75
PASSED THROUGH
≃ 0 %
ORBIT LOSS
≃ 0.15 %
H(r)
R(cm)
0
50
100
150
1
2
3
4
5
6
7
8
9
10

Fig. 8.

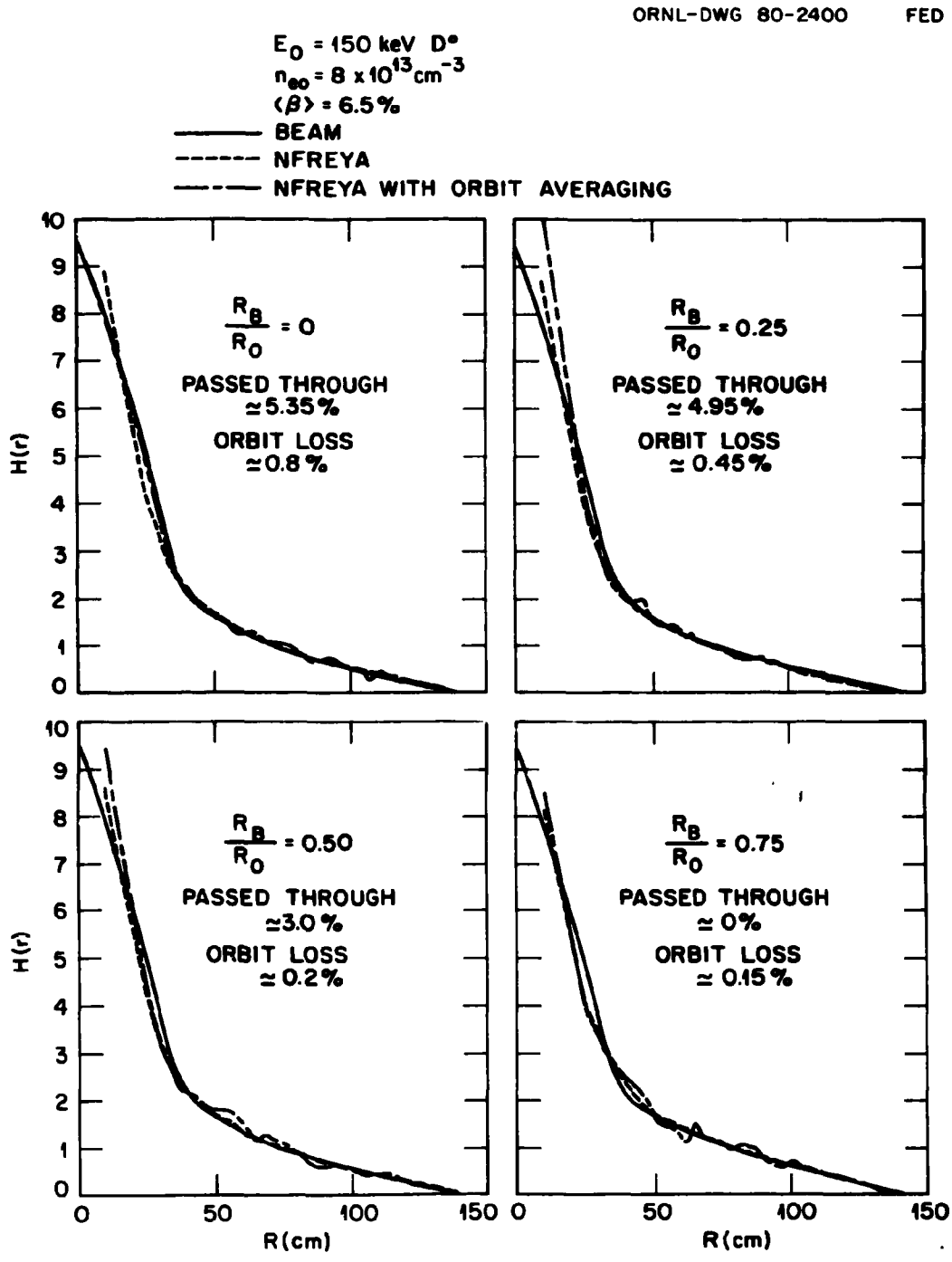
ORNL-DWG 80-2400 FED
E_0 = 150 keV D°
n_{e0} = 8 x 10^{13} cm^{-3}
⟨β⟩ = 6.5%
BEAM
NFREYA
NFREYA WITH ORBIT AVERAGING
$\frac{R_B}{R_0}$ = 0
PASSED THROUGH ≃5.35%
ORBIT LOSS ≃0.8%
$\frac{R_B}{R_0}$ = 0.25
PASSED THROUGH ≃4.95%
ORBIT LOSS ≃0.45%
$\frac{R_B}{R_0}$ = 0.50
PASSED THROUGH ≃3.0%
ORBIT LOSS ≃0.2%
$\frac{R_B}{R_0}$ = 0.75
PASSED THROUGH ≃0%
ORBIT LOSS ≃0.15%
H(r)
R(cm)
0
50
100
150
1
2
3
4
5
6
7
8
9
10

Fig. 9.

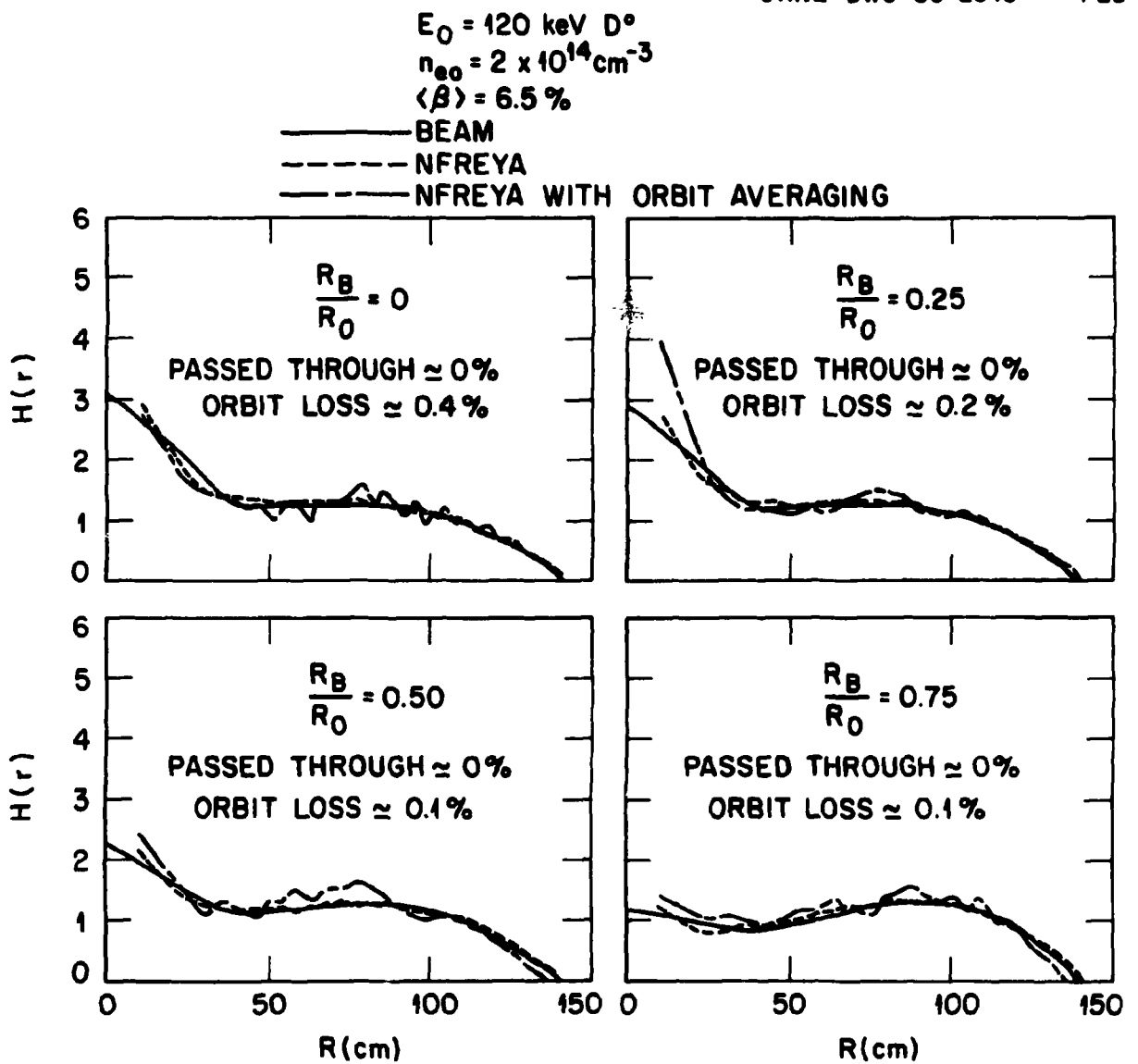
E_0 = 120 keV D°
n_{e0} = 2 x 10^{14} cm^{-3}
⟨β⟩ = 6.5 %
BEAM
NFREYA
NFREYA WITH ORBIT AVERAGING
$\frac{R_B}{R_0}$ = 0
PASSED THROUGH ≃ 0%
ORBIT LOSS ≃ 0.4 %
$\frac{R_B}{R_0}$ = 0.25
PASSED THROUGH ≃ 0%
ORBIT LOSS ≃ 0.2 %
$\frac{R_B}{R_0}$ = 0.50
PASSED THROUGH ≃ 0%
ORBIT LOSS ≃ 0.1 %
$\frac{R_B}{R_0}$ = 0.75
PASSED THROUGH ≃ 0%
ORBIT LOSS ≃ 0.1 %
H(r)
R(cm)
0
50
100
150
1
2
3
4
5
6

Fig. 10.

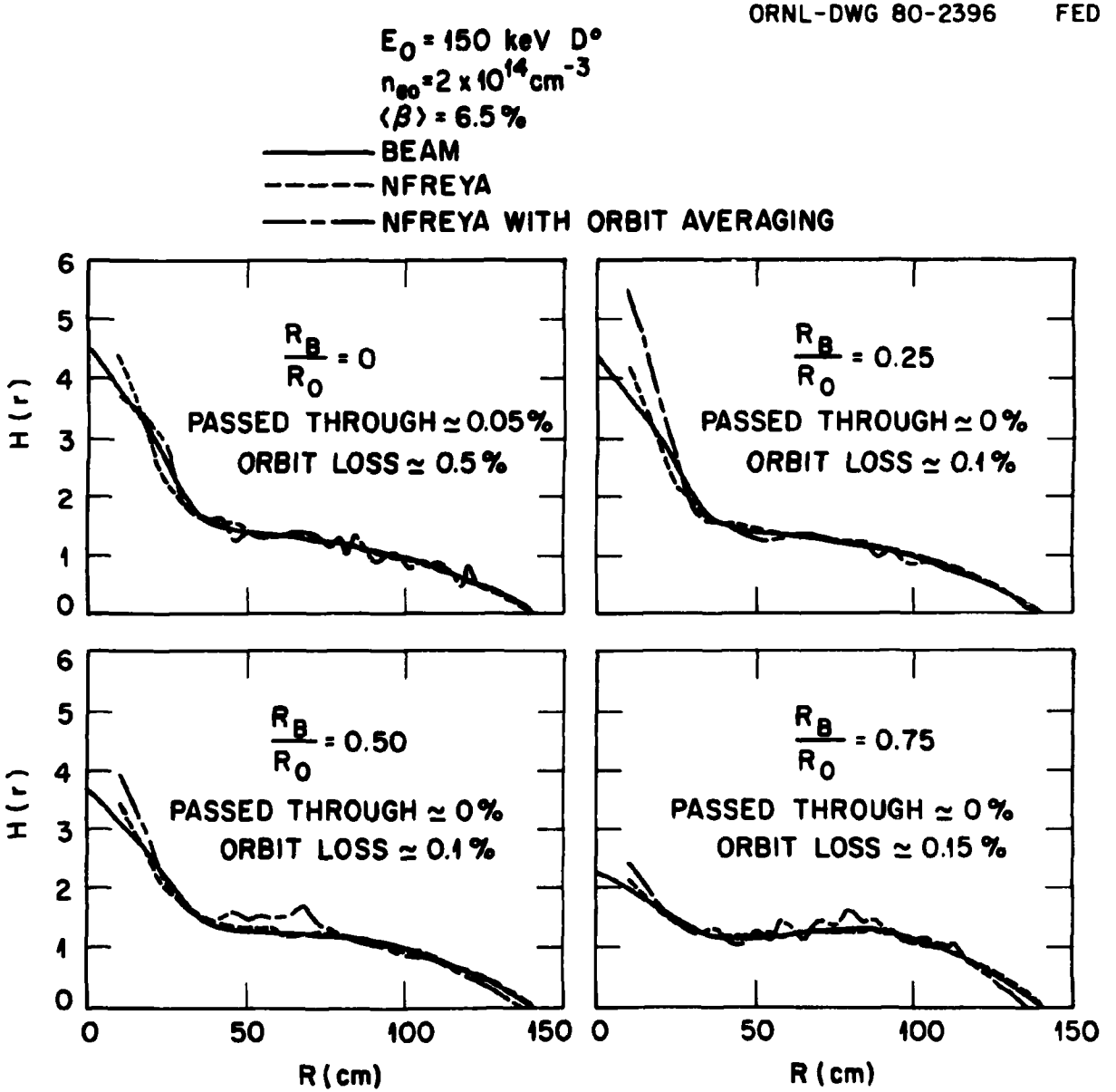
E_0 = 150 keV D°
n_{e0} = 2 x 10^{14} cm^{-3}
⟨β⟩ = 6.5 %
BEAM
NFREYA
NFREYA WITH ORBIT AVERAGING
$\frac{R_B}{R_0}$ = 0
PASSED THROUGH ≃ 0.05%
ORBIT LOSS ≃ 0.5 %
$\frac{R_B}{R_0}$ = 0.25
PASSED THROUGH ≃ 0 %
ORBIT LOSS ≃ 0.1 %
$\frac{R_B}{R_0}$ = 0.50
PASSED THROUGH ≃ 0 %
ORBIT LOSS ≃ 0.1 %
$\frac{R_B}{R_0}$ = 0.75
PASSED THROUGH ≃ 0 %
ORBIT LOSS ≃ 0.15 %
H(r)
R (cm)
0
1
2
3
4
5
6
50
100
150

Fig. 11.

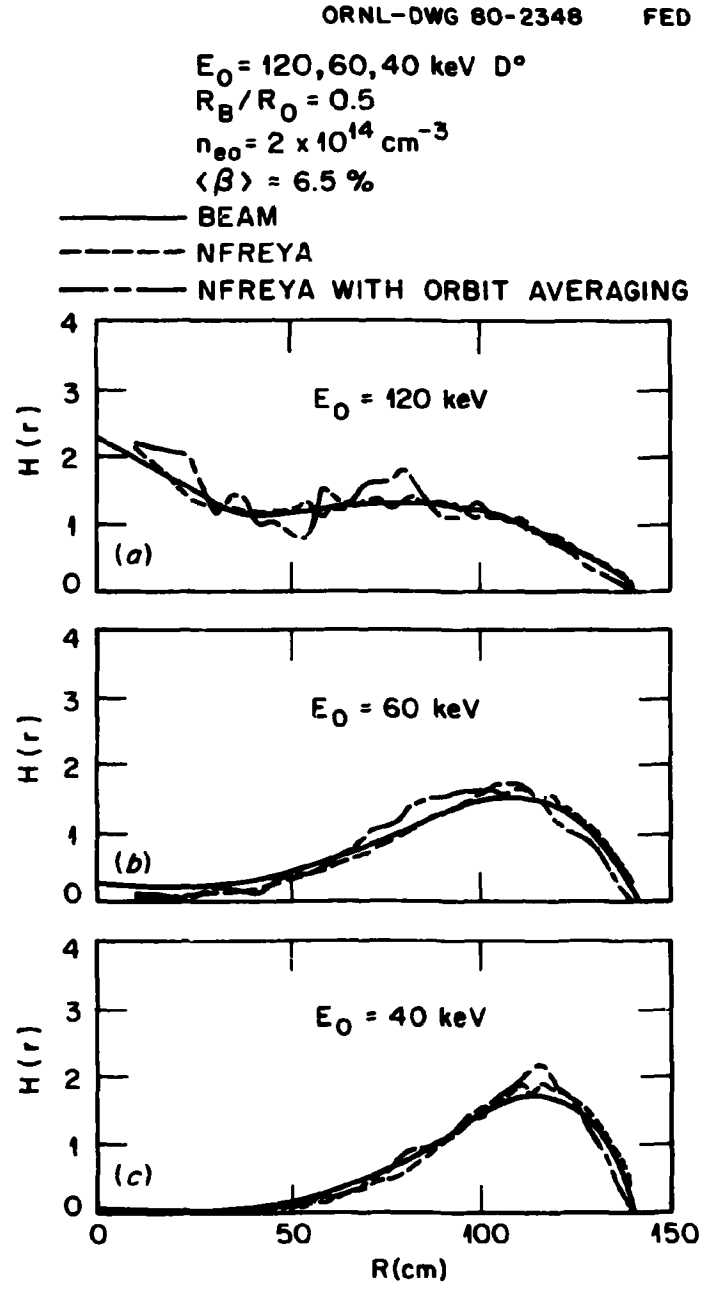
ORNL-DWG 80-2348 FED
E_0 = 120,60,40 keV D°
R_B/R_0 = 0.5
n_{e0} = 2 x 10^{14} cm^{-3}
⟨β⟩ = 6.5 %
BEAM
NFREYA
NFREYA WITH ORBIT AVERAGING
H(r)
E_0 = 120 keV
(a)
E_0 = 60 keV
(b)
E_0 = 40 keV
(c)
0
1
2
3
4
0
50
100
150
R(cm)

Fig. 12.

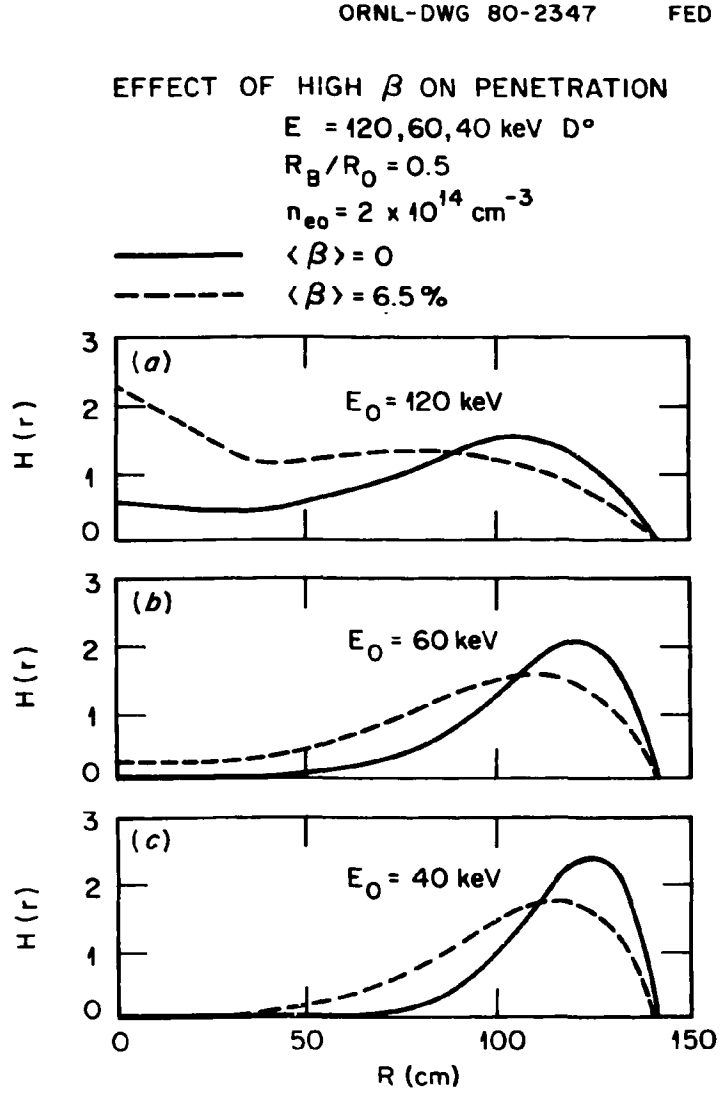
ORNL-DWG 80-2347 FED
EFFECT OF HIGH β ON PENETRATION
E = 120,60,40 keV D°
$R_B/R_0 = 0.5$
$n_{e0} = 2 \times 10^{14}\ cm^{-3}$
⟨β⟩ = 0
⟨β⟩ = 6.5%
(a)
E_0 = 120 keV
(b)
E_0 = 60 keV
(c)
E_0 = 40 keV
H(r)
R (cm)
0
50
100
150
1
2
3

Fig. 13.